

Hybrid Traffic Control and Coordination from Pixels

Michael Villarreal, Bibek Poudel, Jia Pan, Weizi Li

Abstract—Traffic congestion is a persistent problem in our society. Existing methods for traffic control have proven futile in alleviating current congestion levels leading researchers to explore ideas with robot vehicles given the increased emergence of vehicles with different levels of autonomy on our roads. This gives rise to hybrid traffic control, where robot vehicles regulate human-driven vehicles, through reinforcement learning (RL). However, most existing studies use precise observations that involve global information, such as network throughput, as well as local information, such as vehicle positions and velocities. Obtaining this information requires updating existing road infrastructure with vast sensor networks and communication to potentially unwilling human drivers. We consider image observations as the alternative for hybrid traffic control via RL: 1) images are readily available through satellite imagery, in-car camera systems, and traffic monitoring systems; 2) Images do not require a complete re-imagination of the observation space from network to network; and 3) images only require communication to equipment. In this work, we show that robot vehicles using image observations can achieve similar performance to using precise information on networks, including ring, figure eight, merge, bottleneck, and intersections. We also demonstrate increased performance (up to 26%) in certain cases on tested networks, despite only using local traffic information as opposed to global traffic information.

I. INTRODUCTION

Traffic congestion is a prevalent challenge in modern society that causes delays, gridlocks, and substantial economic losses. Traditional traffic management methods such as traffic lights, stop signs, and ramp meters have proven insufficient in alleviating the current level of congestion [1, 2]. As more vehicles with varying degrees of autonomy are introduced into our transportation system, the idea of hybrid traffic control, which involves the use of robot vehicles (RVs) to regulate human-driven vehicles (HVs), is gaining popularity as a solution. Studies have shown the effectiveness of this approach in stabilizing traffic on roads of different configurations, including ring and figure-eight roads [3], merge and bottleneck roads [4], and intersections [4, 5, 6]. Among various control methods for hybrid traffic, reinforcement learning (RL) has emerged as a promising tool, as it can handle the complexity of hybrid traffic behaviors without the need for predefined models or heuristics [7].

Recent research on hybrid traffic control via RL all uses precise information on traffic conditions as input. This means the RV receives both exact global information such as network throughput and travel time as well as exact local information such as surrounding vehicles' positions and velocities. For the RV to receive precise global information, sensor infrastructure to collect this information is required. This involves updating or completely upending existing road networks, which can incur significant costs. To receive precise local information, the

RV needs to establish vehicle-to-vehicle (V2V) and vehicle-to-infrastructure (V2I) communications (where the infrastructure tracks individual vehicles). While V2I also needs augmented infrastructure with proper sensors installed, V2V additionally requires HVs to have the capabilities to send precise information and opt-in to the communication with neither of these being guaranteed. To avoid these pitfalls of using precise observations as input to RL policies, we consider image observations as the alternative. Imagery about traffic conditions is readily available. To start with, satellite imagery can capture traffic conditions in both cities and rural areas where communication is sparse. In addition, our road infrastructure is equipped with ubiquitous camera systems. Examples include Performance Measurement System (PeMS) [8] which monitors city-scale traffic and Advanced Traffic Management System (ATMS) [9] which provides real-time images of traffic conditions. Lastly, many modern cars are installed with cameras that can capture 360° view of the surroundings.

There are also benefits of using image observations to train RL policies for hybrid traffic control. First, using pixels as inputs allows for end-to-end training thus avoiding the need for the manual design of the global and local traffic information. Designing the observation space has been a hurdle for hybrid traffic control via RL: different scenarios need a complete rethinking of what information to extract and how to effectively combine the information. For example, the figure-eight network uses all vehicles' positions and velocities while the bottleneck network uses mean position and velocity of HVs and RVs on user-defined segments combined with network outflow as the observation. Using pixels can further enable RVs to generalize to new situations as the V2I support could vary significantly in different parts of a road network.

This project focuses on exploring the use of image observations as an alternative to precise observations for training RL policies in hybrid traffic control. The image observations, which are centered on RVs, have generic resolutions and provide only local information about the surroundings of RVs and not global information about the entire network. While we still require V2V communication as images are shared amongst the RVs, the use of image observations eliminates the need for HVs to participate in the communication process. This overcomes the uncertainty of having HVs collect and send information and opt-in to share their information. In summary, our contributions are as follows.

- Image observations are used instead of precise observations for training RVs in hybrid traffic control. These images are both generic and only need to record the local surroundings of the RVs. In contrast, global information is needed when using precise observations.

- Demonstration of the same-level performance to using precise observations on ring roads, figure-eight networks, and merge networks.
- Improved performance in certain cases as compared to using precise observations, such as a 26% increase in average vehicle velocity in the merge network and a 6% increase in network outflow in the bottleneck network.

To the best of our knowledge, we are the first in conducting thorough experiments to demonstrate the feasibility of utilizing image observations in hybrid traffic control through RL.

II. RELATED WORK

There are numerous studies demonstrating the use of images or pixel values in reinforcement learning (RL). These applications range from playing Atari games [10, 11, 12] to improving ultrasound images and diagnoses [13, 14]. A series of image trajectories have also been adopted for training RL agents [15, 16, 17]. While these studies highlight the potential of images in RL, the applications differ and our focus is hybrid traffic control via robot vehicles, a multi-agent setting.

A significant portion of training RVs via RL focuses on individual vehicle driving but not controlling the entire traffic [18, 19]. To list some examples, images are used with vision transformers to learn an effective driving policy [20], to train RVs to drive in simulation [21, 22, 23, 24], or to prevent crashes by capturing the RVs' surroundings [25]. In the work by Pan et al. [26], simulated images are transformed into realistic-looking images to train RVs via RL. While these studies apply RL and images to RVs, they do not concentrate on traffic control.

The work by Wu et al. [3] pioneers hybrid traffic control using RL. They show the effectiveness of training an RV on smoothing out stop-and-go waves on a ring road. Further tests are conducted by Vinitsky et al. [4] on additional networks, including merge, bottleneck, and intersection scenarios. Recently, Wang et al. [6] manage to scale up hybrid traffic control to real-world, complex intersections while controlling and coordinating hundreds of vehicles. While significant advancements have been made in hybrid traffic control, all these studies use precise observations as inputs to the RL policy. These precise observations include both global and local traffic conditions, such as network throughput and vehicle position and velocity.

Our work replaces these precise observations with image observations in the training of RL policies for hybrid traffic control. This shift to image observations has several benefits. First, it eliminates the requirement for manual design of the observation space for different traffic scenarios, making it a more flexible solution. Second, it can leverage existing traffic infrastructure as image data is readily available from sources such as satellite imagery, traffic monitoring systems, and vehicle surround-view cameras.

There are several studies exploring hybrid traffic control with images. However, there are key differences between their efforts and ours. To start with, the work by Maske et al. [27] presents a decentralized method for training RVs using

images, but the test is only done on the ring network and the focus is not to prevent stop-and-go waves. The work by Wu and Bayen [28] shows that human driving can be positively augmented using an RL controller trained on local image observations. Their approach is tested on the ring and figure-eight networks. However, again, the focus is not to prevent stop-and-go traffic. To the best of our knowledge, our work is the first to perform extensive experimentation on various road networks to prove the viability of using image observations for RL-based hybrid traffic control in alleviating traffic congestion.

III. METHODOLOGY

In this section, we first introduce our problem formulation and then outline the details (observation, action, and reward) for the five road networks in which we conduct experiments. We also provide details on precise observations [3, 4] and compare their differences to image observations.

A. Preliminaries

We model the RL problem as a Partially Observable Markov Decision Process (POMDP) represented by a tuple $(\mathcal{S}, \mathcal{A}, \mathcal{P}, \mathcal{R}, p_0, \gamma, T, \Omega, \mathcal{O})$ where: \mathcal{S} is the state space; \mathcal{A} is the action space; $\mathcal{P}(s'|s, a)$ is the transition probability function; \mathcal{R} is the reward function; p_0 is the initial state distribution; $\gamma \in (0, 1]$ is the discount factor; T is the episode length (horizon); Ω is the observation space; and \mathcal{O} is the probability distribution of retrieving an observation $\omega \in \Omega$ from a state $s \in \mathcal{S}$.

At each timestep $t \in [1, T]$, a robot vehicle (RV) uses its policy $\pi_\theta(a_t|s_t)$ to take an action $a_t \in \mathcal{A}$, given the state $s_t \in \mathcal{S}$. The RV's environment provides feedback on action a_t by calculating a reward r_t and transitioning the agent into the next state s_{t+1} . The RV's goal is to learn a policy π_θ that maximizes the discounted sum of rewards, i.e., return, $R_t = \sum_{i=t}^T \gamma^{i-t} r_i$. We use Proximal Policy Optimization [29], a model-free, on-policy algorithm, to learn the optimal policy.

B. Road Network MDPs

We train RVs using RL on five road networks (ring, figure eight, intersection, bottleneck, and merge) shown in Fig. 1 using image observations. We give a brief environment description and outline MDP details, such as observation space, action space, and reward function, for each network and compare the differences between precise observations and image observations. Further details related to these networks are provided in Section IV.

1) *Ring Network*: The ring network is a widely used benchmark in traffic control. A single-lane circular road network consisting of 22 vehicles with 21 human-driven vehicles (HVs) and one RV is considered. It simulates how subtle perturbations due to imperfections in human driving behavior can amplify and propagate, leading to an eventual standstill for some vehicles. This situation is known as 'stop-and-go traffic' which acts as a wave that propagates continually through the ring, opposite the direction of travel. The RV's goal is to

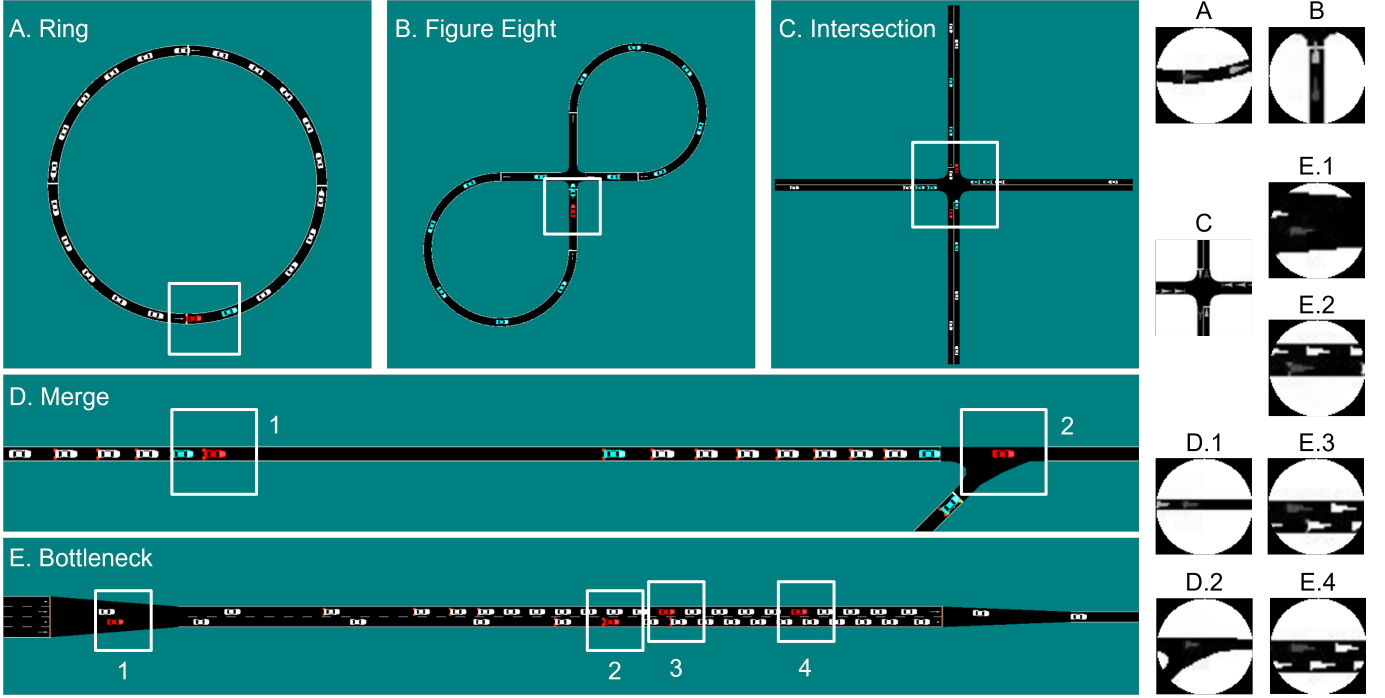


Fig. 1. We experiment on five road networks: ring, figure eight, intersection, merge, and bottleneck. The image observations used for each road network are presented on the right. The car shapes in the color figures are for visualization-purpose only. Human-driven vehicles (HVs) are white, observed HVs (when using precise observations) are blue, and robot vehicles (RVs) are red. All HVs are blue when using image observations to provide contrast from a white background as seen in the image observations. No HV is blue in the bottleneck network as specific HVs are not observed, but rather information about the entire network. We use static, grayscale, 84×84 images centered over RVs (or intersection for the intersection network) that provide only local information to RVs. Ring, figure eight, and intersection use a single image, while merge and bottleneck use five and 15, respectively.

dampen these waves, thus increasing the average velocity of all vehicles.

Observation Space. Every timestep, our observation is a gray-scale image of dimensions 84×84 pixels, centered on a single RV as shown in Fig. 1, right A. To simulate limited visibility, the image is masked by a circle with a radius corresponding to 28.75 meters in real world.

Precise observations are a vector of the RV’s velocity, the difference between the leading vehicle’s velocity and the RV’s velocity, and the difference between the leading vehicle’s position and the RV’s position. The positions of the vehicles are defined relative to the ring network, and all three values are normalized. These observations have been used previously [3] to produce state-of-the-art performance.

Action Space. The action is defined as a continuous distribution space of acceleration bound by $[-1, 1]$ m/s².

Reward. The reward function encourages high average velocity of all vehicles while penalizing accelerations (control action) above a threshold:

$$r = \begin{cases} 0, & \text{if collision,} \\ \lambda_1 * v/20 + A, & \text{otherwise,} \end{cases} \quad (1)$$

where λ_1 is empirically set to 4, v is the average velocity of all vehicles, and A is

$$A = \begin{cases} 0, & \text{if } a > \phi, \\ \lambda_2 * (\phi - a), & \text{otherwise.} \end{cases} \quad (2)$$

In A, λ_2 is empirically set to 3, a is the average of accelerations, and ϕ is a threshold value set to 0. The RV is punished for accelerating when a is positive.

2) *Figure Eight Network:* The figure-eight network simulates an intersection in a closed loop with 14 vehicles—13 HVs and one RV. As a result of its shape and the fixed number of vehicles in the network, queues form among cars that try to cross the intersection. This causes a network-wide decrease in average vehicle velocity. The RV’s goal is then to increase the average velocity of all vehicles in the network.

Observation Space. Our observation is the same as of the ring network (see Sec. III-B1). An example is given in Fig. 1, right B. The dimension of the masked circle corresponds to a 21.25 m radius. Precise observations are a vector of the velocities and positions of all vehicles within the figure-eight network, including RV and HVs [3]. This complete information reflects that the state space is used. As our observations are local, i.e., images centered on the RV, learning an optimal policy includes extra steps of perception and representation learning, making it much more challenging than with precise observations.

Action Space. The action is defined in a continuous distribution of accelerations bound by $[-3, 3]$ m/s².

Reward. The objective of the RV is to increase the velocities of all vehicles in the network:

$$r = \frac{\max(\|v_{des} * 1^k\|_2 - \|v_{des} - v\|_2, 0)}{\|v_{des} * 1^k\|_2}, \quad (3)$$

where v_{des} (desired velocity) is 10 m/s, v is a vector of all vehicles' velocities, and k is the total number of vehicles in the network.

3) *Intersection Network*: This network represents an unsignalized intersection where east/westbound traffic flow is less than north/southbound traffic flow. The difference in flows is significant enough such that east/westbound traffic forms queues as it would otherwise be unsafe to cross the intersection. This intersection functions similarly to an idealized two-way stop for the east/west traffic. RVs are placed in the north/south directions with a penetration rate of 20%. The RVs' objective is the minimization of queues forming and increased average vehicle velocity along the east/west directions. This environment allows for studying hybrid traffic control in directions absent of RVs since RVs control only the north/south directions.

Observation Space. Our observation is an 84×84 , grayscale image (shown in Fig. 1, right C) taken at the intersection's center. The image observations focus on the intersection. No circle mask is applied to the images. The image dimensions correspond to a square with a side length of 50 m in real world.

Precise observations include global traffic information as well as local traffic information. Vehicles closest to the intersection up to a user-defined number are considered [3, 4]. Specifically, the observation space has the following information: the velocities of each vehicle, the position distance to the intersection of each vehicle, the edge number of each vehicle (this identifies if the vehicle is in east/west traffic or in north/south traffic), the density of the edges, and the average vehicle velocity of the edges. Our RVs cannot infer network-wide information from the limited radius observations making learning more difficult.

Action Space. The actions are defined in a continuous distribution of accelerations in the range $[-7, 7]$ m/s² where each RV receives an acceleration value. At most five RVs take actions, although more or less RVs can be present in the network. If there are less, the remaining acceleration values are not used. If there are more, extra RVs act as HVs.

Reward. As the RVs' objective is to reduce queue length and increase average vehicle velocity in east/west bound traffic, the reward function penalizes both vehicle delay and vehicle standstills in traffic:

$$r = -(D + SS), \quad (4)$$

where D is

$$\frac{t * \sum((sl - v)/sl)}{k + eps}, \quad (5)$$

and t is the current timestep, sl is a vector of speed limits for each edge of the network, v is a vector of velocities for each vehicle in the network, k is the number of vehicles in the network, and eps prevents division by zero. The function SS is

$$SS = gain * num_{ss}, \quad (6)$$

where $gain$ is 0.2 and num_{ss} is the number of standstill vehicles. Given the reward is negative, the RVs' goal is to minimize delay and standstill of the vehicles.

4) *Merge Network*: The merge network contains a highway and an on-ramp. The highway and on-ramp respective flows can create stop-and-go waves along the highway and congest the on-ramp, reducing the average velocity and outflow. The RVs' goal is to minimize the formation of such waves and increase average vehicle velocity. RVs are only placed on the highway at a penetration rate of 10%

Observation Space. Our observation is a stack of five images, each of size 84×84 (shown in Fig 1, right D), centered on the RV. There can be multiple RVs present at any given time. However, we observe that five is the maximum. If there are less than five RVs present, the remaining stack is padded with black images; if more, the extra RVs are treated as HVs. The image dimensions correspond to 41.25 m in real world.

Precise observations are a vector of the following [3, 4]: the velocities of the following and leading vehicle for each RV; the difference in positions between the RV and the following and leading vehicles; and the velocity of each RV. HVs on the on-ramp are observed only if they are following vehicles or have merged onto the highway.

Action Space. The actions are defined in a continuous distribution of accelerations bounded by $[-1.5, 1.5]$ m/s². If there are more than five RVs, the additional RVs act as HVs. If there are less, then the leftover RL actions are not used.

Reward. The objective of the RVs is to improve the overall vehicle velocity and increase the outflow of the network:

$$r = \frac{\max(\|v_{des} * 1^k\|_2 - \|v_{des} - v\|_2, 0)}{\|v_{des} * 1^k\|_2} - H, \quad (7)$$

where

$$H = \alpha \sum_{i \in RVs} \max[h_{max} - h_i(t), 0], \quad (8)$$

and h_{max} is empirically set to 1 and $h_i(t)$ is the headway of an RV at t . The first term is Eq. 3, which is trying to improve the overall vehicle velocity. The objective of H is to penalize small headways between an RV and an HV to discourage traffic bunching up and potentially causing stop-and-go waves.

5) *Bottleneck Network*: The bottleneck network simulates vehicles experiencing capacity drop [30] where a network's outflow significantly decreases after the network inflow surpasses a threshold. The goal of the RVs is to improve outflow. The bottleneck network represents a bridge with lanes decreasing from $4 \times l$ to $2 \times l$ to l (where l is a scaling factor and is one for our work). The penetration rate of the RV is 10%.

Observation Space. Our observation consists of 15 stacked images, each of size 84×84 (shown in Fig. 1 right E), as a maximum of 15 RVs are placed in the network. If there are less than 15 RVs, the remaining stack is filled with black images; if more than 15 RVs, additional RVs are treated as HVs. The image dimensions correspond to a circle with a radius of 25 m in real world.

Precise observations are a vector comprised of the following [3, 4]: the mean positions and velocities of all human drivers for each lane for each user-defined segment of the road network; the mean positions and velocities of the RVs for each user-defined segment of the road network (unlike HVs, the lanes RVs are present on are not tracked); and the outflow of the network (veh/hr) over the last five seconds. This observation is difficult to design as it consists of both microscopic and macroscopic traffic statistics. In addition, since it focuses on segments of the bottleneck rather than individual vehicles, it can be considered as global information. In contrast, our observations only need to contain local information.

Action Space. Unlike the previously defined environments where the action is acceleration, here the action is defined as velocity in the range $[0.01, 23]$ m/s. If there are less than 15 RVs, the outstanding RL actions are not used; if more, the extra RVs assume the role of HVs.

Reward. The objective is to increase the outflow of the network and reduce the frequency of capacity drops:

$$r_t = \sum_{i=t-\frac{5}{\Delta t}}^{i=t} \frac{N_{exit}(i)}{5(\Delta t * N_{lanes} * 500)}, \quad (9)$$

where $N_{exit}(i)$ is the number of vehicles that left the network at timestep i over the last five seconds, Δt is the simulation timestep, and N_{lanes} is number of lanes.

IV. EXPERIMENTS AND RESULTS

In this section, we present our experimental setup and detail the training and evaluation results obtained for each tested road network using both image and precise observations.

A. Experiment Setup

We train RVs using the Proximal Policy Optimization (PPO) [29], with hyperparameters given in Table I. The HVs are operated by Intelligent Driver Model (IDM) [31] with stochastic noise in the range $[-0.2, 0.2]$ added to account for heterogeneous driving behaviors. RVs are trained for 200 episodes. Table II provides further simulation details. Warmup refers to the number of timesteps before the activation of RL policies. Horizon refers to the episode length and Δt is the simulation timestep.

Trained policies in each network are evaluated for 10 rollouts, and results are presented as averages. Convolutional Neural Networks with filters (formatted as [out channels, kernel size, stride]) of $[16, 8, 4]$, $[32, 4, 2]$, and $[256, 11, 1]$ are adopted. Experiments are conducted using i7-12700k CPU with 32G RAM.

B. Results

1) *Ring Network:* The ring network hosts 21 HVs and one RV where the RV's objective is to remove stop-and-go waves. At initialization, the 22 vehicles are uniformly placed from each other and act as HVs for 3000 warmup timesteps. During this period, stop-and-go waves will form and persist. Afterwards, the RV is activated for 3000 timesteps. During training, the RV is trained on rings with circumference

TABLE I
HYPERPARAMETERS OF PPO [29] USED IN OUR EXPERIMENTS.

Hyperparameter	Value
Minibatch Size	128
Clipping	0.3
γ	0.999
λ	0.97
KL Initialization	0.2
KL Target	0.02
Value Function Coefficient	1.0
Entropy Coefficient	0.0
Learning Rate	5e-05

TABLE II
SIMULATION SETTINGS FOR THE DIFFERENT ROAD NETWORKS. Δt IS THE SIMULATION TIMESTEP. WARMUP IS THE TIMESTEP DURATION WHERE RVs ACT AS HVs, AND HORIZON IS THE TIMESTEP DURATION WHERE RVs TRANSITION TO NEW STATES AND TAKE ACTIONS USED FOR LEARNING.

Network	Δt	Warmup	Horizon
Ring	0.1	3000	3000
Figure Eight	0.1	0	1500
Intersection	0.1	0	400
Bottleneck	0.5	40	1000
Merge	0.5	0	750

sampled uniformly from $[220, 270]$. For testing, this range is extended to $[210, 290]$.

The results are shown in Fig. 2 TOP-LEFT. Our approach using image observations is represented in blue, while the result of using precise observations is represented in orange. The vertical lines represent the bounds for what densities (converted from the ring length) are seen during training. Our results show, at all densities tested, the RV with image observations is able to prevent stop-and-go waves and achieve the same-level performance as of using precise observations.

Fig. 3 shows the time-space diagram of all vehicles over an episode. The shockwaves from 200 to 300 seconds (one second equals 10 timesteps) reflect stop-and-go traffic. After 300 seconds, the image-trained RV starts taking action. With an initial period of acceleration, the RV then stabilizes the traffic. For this demonstration, the horizon is set to 5000 timesteps (500 seconds) to illustrate the generalizability of our approach beyond the training horizon.

2) *Figure Eight Network:* The figure-eight network is comprised of 13 HVs and one RV driving with no warmup and a horizon of 1500 timesteps. The efficacy of a trained RV is measured by the average vehicle velocity in the network. Previously, the RV is trained only on a single, inner-loop radius [3] (inner-loop radius is used to calculate the overall network length), but we expand the scenario by training on the range $[20, 30]$ m and expand this range to $[18, 32]$ m during

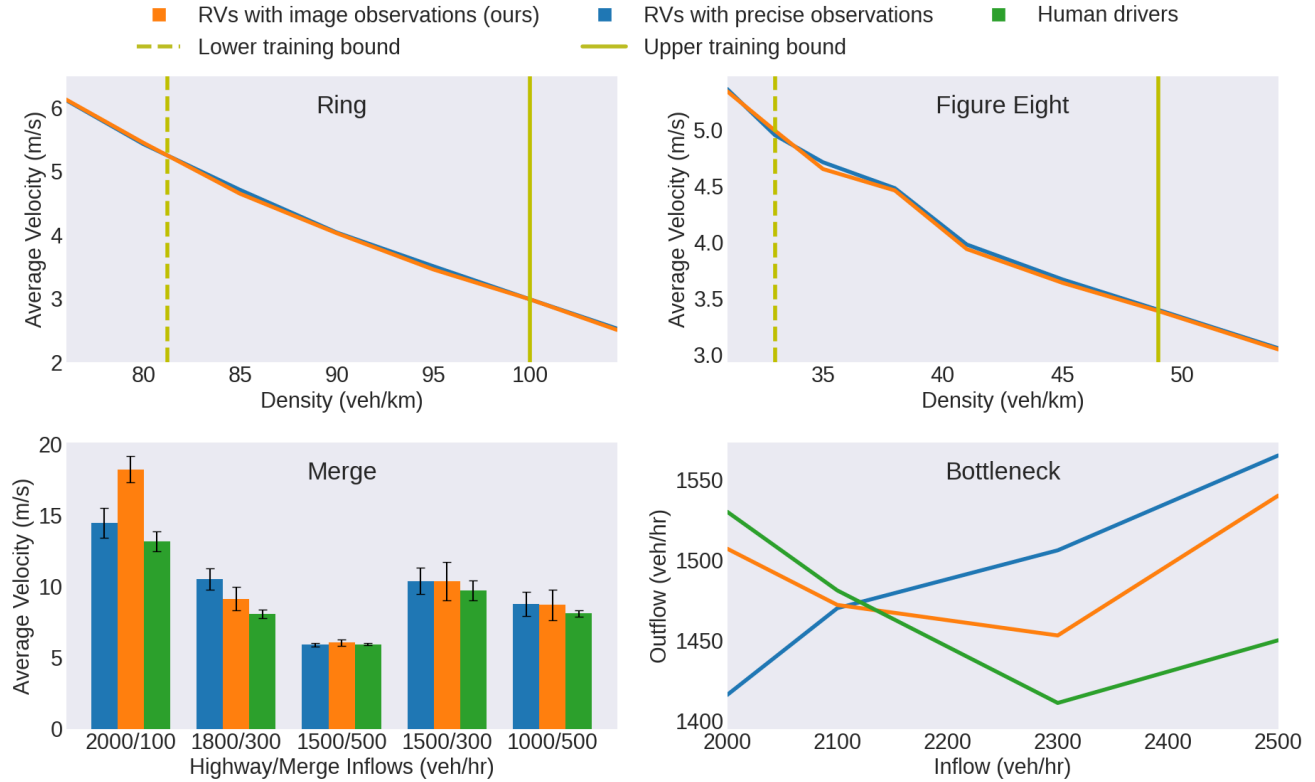


Fig. 2. Results for the ring, figure eight, merge, and bottleneck networks. TOP-LEFT: An RV with image observations achieves the same performance as an RV with precise observations. Stop-and-go waves are prevented at all densities. TOP-RIGHT: Similar to the ring network, an RV with image observations achieves hybrid traffic control comparable to an RV with precise observations. BOTTOM-LEFT: In a majority of scenarios, RVs with image observations achieve similar performance as RVs with precise observations. In the 2000/100 inflows scenario, the RVs using image observations even surpass the performance of the RVs using precise observations by 26%. BOTTOM-RIGHT: RVs with image observations outperform the performance of RVs with precise observations at 2000 inflow by 6%, but in general, the performance is lower, which is likely due to the absence of global information in the image observations.

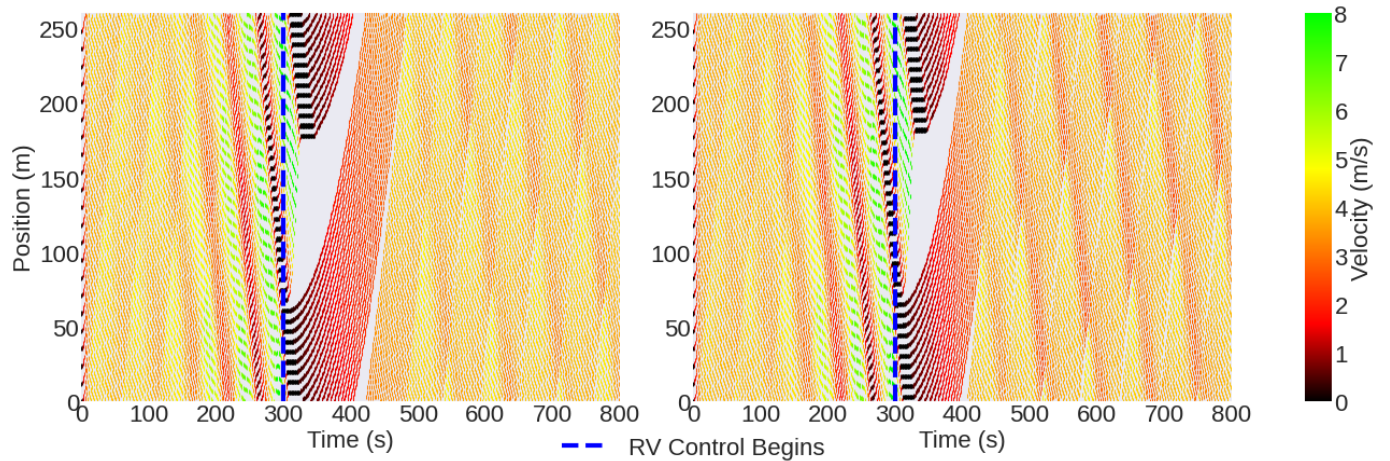


Fig. 3. Time-space diagrams showing stop-and-go waves being prevented after RVs start taking action. The experiments are conducted on the ring network with a length of 260 m. Stop-and-go waves form around 200 to 300 seconds (10 timesteps equals one second). LEFT: An RV trained on image observations is able to prevent stop-and-go waves once it begins taking actions similar to an RV trained on precise observations; RIGHT: An RV trained with only position information (without velocity information) can also prevent stop-and-go waves.

TABLE III
RESULTS FOR INTERSECTION NETWORK. AVERAGE VELOCITY IS THE MEAN VELOCITY OF VEHICLES TRAVELING EAST/WESTBOUND, AND QUEUE LENGTH IS THE NUMBER OF CARS WAITING TO CROSS THE INTERSECTION IN THE EAST OR WEST DIRECTIONS.

	Average Velocity (m/s)	Queue Length
Human Drivers	3.70 ± 0.00	5 vehicles
Precise Obs.	5.90 ± 0.23	3 vehicles
Image Obs.	4.75 ± 0.02	3 vehicles

evaluation.

Our results are shown in Fig. 2 TOP-RIGHT. We evaluate on average vehicle velocity at different network densities. The ability to perform hybrid traffic control of an RV with image observations is the same as an RV with precise observations, despite that the image-trained RV only receives local information while the counterpart receives complete global information.

3) *Intersection Network*: In the intersection network, north/south traffic inflow is set to 1333 vehicles per hour (veh/hr) and east/west inflow is set to 500 veh/hr. The RVs' objective is to minimize queue length and increase the average velocity of traffic along the east/west directions, where queues form.

Results are shown in Table III where we examine the average velocity of all vehicles and queue lengths along the east/west directions. RVs with image observations can provide similar performance to RVs with precise observations in regard to queue length. The average vehicle velocity of RVs with image observations is less than RVs with precise observations. We believe this performance difference is due to precise global observations knowing exactly what edges vehicles are on and their corresponding velocities, which allow the RVs to know when HVs are at standstill in the east/west directions. Both RV types outperform HVs in both evaluation metrics.

Fig. 4 illustrates the development of queues with only HVs versus RVs with image observations. The southbound RV in the right image is slowing down momentarily, which allows east/westbound HVs to safely cross the intersection. With only HVs, they travel at velocities that cause queues in the east/west directions to develop.

4) *Merge Network*: The merge network simulates vehicles entering a highway from an on-ramp. This experiment evaluates on a set of five combinations of highway/merge inflow rates: $\{2000/100, 1800/300, 1500/500, 1500/300, 1000/500\}$. The different inflow combinations result in varying levels of congestion due to vehicles merging onto the highway. In either case, stop-and-go waves form on the highway, resulting in decreased average velocity of all vehicles. This combination of inflows has not been previously studied, except for the 2000/100 inflow rates [3, 4].

Fig. 2 BOTTOM-LEFT presents our results. HVs' performance is provided for comparison. RVs with image obser-

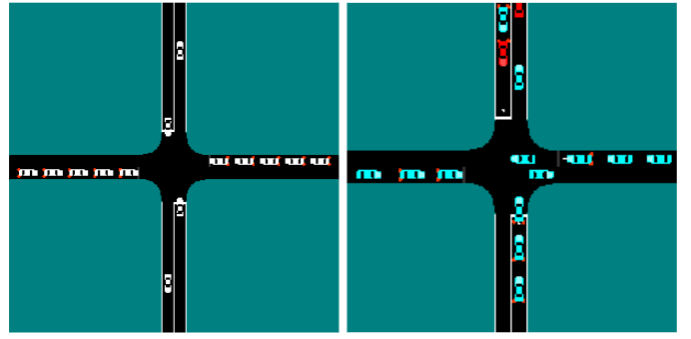


Fig. 4. Queue length comparison between all HVs and hybrid traffic on the intersection network. LEFT: With only HVs, the queue length is five (in both east/west directions) by episode termination. North/southbound HVs travel at speeds that allow safe crossing infrequently causing queue growth over time. RIGHT: With RVs, the queue length is only three by episode termination. This shows that RVs can assist traffic on lanes where they are not present. Note that HVs are blue, instead of white.

ations have similar performance to RVs with precise observations at 1500/300 and 1000/500 inflows rates. The latter outperforms the former in the 1800/300 inflows scenario, but the former (our approach) outperforms the latter in the 1500/500 and 2000/100 inflows scenarios. RVs with image observations provide the largest performance improvement with a 3.79 m/s—a 26% increase—over using precise observations in the 2000/100 scenario. The 1500/500 scenario is difficult to learn on, evidenced by both RV types not being able to outperform HVs. In fact, RVs with precise observations slightly underperform compared to HVs.

5) *Bottleneck Network*: The bottleneck network investigates hybrid traffic control on a bridge with decreasing lane capacity forming a bottleneck at the end. The RVs' objective is to improve outflow (vehicles exiting the network per hour) at the bottleneck. A set of four inflows is tested, i.e., $\{2000, 2100, 2300, 2500\}$, with the goal to capture moderate to severe congestion levels. The range is chosen to demonstrate the congestion effects on the system, while still allowing for potential improvement through hybrid traffic control.

Results for bottleneck are presented in Fig. 2 BOTTOM-RIGHT. At 2000 inflow, image-trained RVs significantly outperform RVs with precise observations by 6%. At 2300 and 2500 inflow rates, RVs with precise observations outperform our approach. A crossover point occurs around 2100, where HVs start to perform worse than RVs. At lower inflows, HVs' performance is higher than RVs suggesting that RVs may hinder network performance by attempting to alleviate congestion that is not present. The bottleneck scenario experiences high levels of congestion throughout the network. We hypothesize this is the reason that causes our approach to underperform precise-trained RVs, since the image observations do not contain network-wide traffic information.

6) *Position-only Observation Space*: We conduct additional experiments to test position-only observations in training RVs under precision information. The purpose of this experiment is to analyze whether RVs can still be leveraged to alleviate traf-

fic congestion given only static positional information, which is similar to positional inference using image observations. This experiment is conducted on the ring network. The observation space changes to a vector of the difference between the RV's position and the leading vehicle's position. Fig. 3 RIGHT shows the time-space diagram for this experiment. As a result, an RV with only position information can achieve the same level of performance as of using complete information (i.e., both position and velocity). This result further solidifies our approach to using image observations without explicitly including the velocity information.

V. CONCLUSION

In this work, we demonstrate the ability of robot vehicles (RVs) to perform hybrid traffic control using reinforcement learning (RL) policies trained on image observations. We examine RVs trained on image observations in five different scenarios: ring, figure eight, intersection, bottleneck, and merge. Additionally, we expand on the figure eight network by training the RL policies on a range of network lengths, and we expand the bottleneck and merge networks by training and testing on inflow rates previously untested. We show that RVs trained on image observations have competitive performances to RVs trained on precise observations.

The use of image observations enables the adoption of existing infrastructure rather than developing a complex, interconnected sensor network that incurs significant costs for our road networks. In addition, our approach allows for end-to-end training of hybrid traffic control. This overcomes the challenge of manually designing the observation space for incorporating various global and local traffic information, which has been an obstacle to training hybrid traffic on heterogeneous road networks.

A. Assumptions About RVs

Note that we do not assume our RVs to be fully autonomous vehicles with equipment and sensors to allow for complete control. Our RVs control only their acceleration (or velocity), which can be achieved by controlling the throttle signal through a control mechanism, using images that do not require significant computational resources to process and receive actions from.

B. Future Work

In the future, we aim to advance this study in several directions. First, we are interested in testing our approach in more complex and larger scenarios [32, 33], which can be calibrated using mobile data to reflect real-world traffic conditions [34, 35, 36]. Second, we would like to incorporate additional generic information such as traffic state predictions [37, 38] and vehicle trajectories [39, 40] into our observation space for potential improvement. Third, we want to improve the resilience of our approach by taking adversarial attacks [41, 42, 43] into account. Lastly, we are interested in studying hybrid traffic control under other mobility-related topics such as traffic safety [44] and micromobility [45].

REFERENCES

- [1] Phil Goodwin. The economic costs of road traffic congestion. 2004.
- [2] Richard Arnott and Kenneth Small. The economics of traffic congestion. *American scientist*, 82(5):446–455, 1994.
- [3] Cathy Wu, Aboudy Kreidieh, Kanaad Parvate, Eugene Vinitsky, and Alexandre M Bayen. Flow: Architecture and benchmarking for reinforcement learning in traffic control. *arXiv preprint arXiv:1710.05465*, 10, 2017.
- [4] Eugene Vinitsky, Aboudy Kreidieh, Luc Le Flem, Nishant Kheterpal, Kathy Jang, Cathy Wu, Fangyu Wu, Richard Liaw, Eric Liang, and Alexandre M Bayen. Benchmarks for reinforcement learning in mixed-autonomy traffic. In *Conference on robot learning*, pages 399–409. PMLR, 2018.
- [5] Zhongxia Yan and Cathy Wu. Reinforcement learning for mixed autonomy intersections. In *2021 IEEE International Intelligent Transportation Systems Conference (ITSC)*, pages 2089–2094. IEEE, 2021.
- [6] Dawei Wang, Weizi Li, Lei Zhu, and Jia Pan. Learning to control and coordinate hybrid traffic through robot vehicles at complex and unsignalized intersections. *arXiv preprint arXiv:2301.05294*, 2023.
- [7] Fang-Chieh Chou, Alben Rome Bagabaldo, and Alexandre M Bayen. The lord of the ring road: a review and evaluation of autonomous control policies for traffic in a ring road. *ACM Transactions on Cyber-Physical Systems (TCPS)*, 6(1):1–25, 2022.
- [8] State of California Department of Transportation. Caltrans pems. <http://pems.dot.ca.gov/>, 2022.
- [9] Colorado Springs ATMS. Advanced traffic management system. <https://coloradosprings.gov/traffic-and-transportation-engineering/page/traffic-management/>, 2022.
- [10] Marc G Bellemare, Yavar Naddaf, Joel Veness, and Michael Bowling. The arcade learning environment: An evaluation platform for general agents. *Journal of Artificial Intelligence Research*, 47:253–279, 2013.
- [11] Volodymyr Mnih, Koray Kavukcuoglu, David Silver, Alex Graves, Ioannis Antonoglou, Daan Wierstra, and Martin Riedmiller. Playing atari with deep reinforcement learning. *arXiv preprint arXiv:1312.5602*, 2013.
- [12] Lukasz Kaiser, Mohammad Babaeizadeh, Piotr Milos, Blazej Osinski, Roy H Campbell, Konrad Czechowski, Dumitru Erhan, Chelsea Finn, Piotr Kozakowski, Sergey Levine, et al. Model-based reinforcement learning for atari. *arXiv preprint arXiv:1903.00374*, 2019.
- [13] Farhang Sahba, Hamid R Tizhoosh, and Magdy MA Salama. A reinforcement learning framework for medical image segmentation. In *The 2006 IEEE international joint conference on neural network proceedings*, pages 511–517. IEEE, 2006.
- [14] Hanane Alloui, Mazin Abed Mohammed, Narjes Benameur, Belal Al-Khateeb, Karrar Hameed Abdulkareem,

- Begonya Garcia-Zapirain, Robertas Damaševičius, and Rytis Maskeliūnas. A multi-agent deep reinforcement learning approach for enhancement of covid-19 ct image segmentation. *Journal of personalized medicine*, 12(2):309, 2022.
- [15] Danijar Hafner, Timothy Lillicrap, Jimmy Ba, and Mohammad Norouzi. Dream to control: Learning behaviors by latent imagination. *arXiv preprint arXiv:1912.01603*, 2019.
- [16] Danijar Hafner, Timothy Lillicrap, Ian Fischer, Ruben Villegas, David Ha, Honglak Lee, and James Davidson. Learning latent dynamics for planning from pixels. In *International conference on machine learning*, pages 2555–2565. PMLR, 2019.
- [17] Manuel Watter, Jost Springenberg, Joschka Boedecker, and Martin Riedmiller. Embed to control: A locally linear latent dynamics model for control from raw images. *Advances in neural information processing systems*, 28, 2015.
- [18] Yu Shen, Weizi Li, and Ming C. Lin. Inverse reinforcement learning with hybrid-weight trust-region optimization and curriculum learning for autonomous maneuvering. In *IEEE/RSJ International Conference on Intelligent Robots and Systems (IROS)*, pages 7421–7428, 2022.
- [19] Bibek Poudel, Thomas Watson, and Weizi Li. Learning to control dc motor for micromobility in real time with reinforcement learning. In *IEEE International Conference on Intelligent Transportation Systems (ITSC)*, pages 1248–1254, 2022.
- [20] Eshagh Kargar and Ville Kyrki. Vision transformer for learning driving policies in complex multi-agent environments. *arXiv preprint arXiv:2109.06514*, 2021.
- [21] Alexey Dosovitskiy, German Ros, Felipe Codevilla, Antonio Lopez, and Vladlen Koltun. Carla: An open urban driving simulator. In *Conference on robot learning*, pages 1–16. PMLR, 2017.
- [22] Peide Cai, Sukai Wang, Hengli Wang, and Ming Liu. Carl-lead: Lidar-based end-to-end autonomous driving with contrastive deep reinforcement learning. *arXiv preprint arXiv:2109.08473*, 2021.
- [23] Óscar Pérez-Gil, Rafael Barea, Elena López-Guillén, Luis M Bergasa, Carlos Gomez-Huelamo, Rodrigo Gutiérrez, and Alejandro Diaz-Diaz. Deep reinforcement learning based control for autonomous vehicles in carla. *Multimedia Tools and Applications*, 81(3):3553–3576, 2022.
- [24] Zhejun Zhang, Alexander Liniger, Dengxin Dai, Fisher Yu, and Luc Van Gool. End-to-end urban driving by imitating a reinforcement learning coach. In *Proceedings of the IEEE/CVF international conference on computer vision*, pages 15222–15232, 2021.
- [25] Zhangjie Cao, Erdem Bıyık, Woodrow Z Wang, Allan Raventos, Adrien Gaidon, Guy Rosman, and Dorsa Sadigh. Reinforcement learning based control of imitative policies for near-accident driving. *arXiv preprint arXiv:2007.00178*, 2020.
- [26] Xinlei Pan, Yurong You, Ziyang Wang, and Cewu Lu. Virtual to real reinforcement learning for autonomous driving. *arXiv preprint arXiv:1704.03952*, 2017.
- [27] Harshal Maske, Tianshu Chu, and Uroš Kalabić. Large-scale traffic control using autonomous vehicles and decentralized deep reinforcement learning. In *2019 IEEE Intelligent Transportation Systems Conference (ITSC)*, pages 3816–3821. IEEE, 2019.
- [28] Fangyu Wu and Alexandre M. Bayen. Cscrs road safety fellowship report: A human-machine collaborative acceleration controller attained from pixel learning and evolution strategies.
- [29] John Schulman, Filip Wolski, Prafulla Dhariwal, Alec Radford, and Oleg Klimov. Proximal policy optimization algorithms. *arXiv preprint arXiv:1707.06347*, 2017.
- [30] Meead Saberi and Hani S Mahmassani. Empirical characterization and interpretation of hysteresis and capacity drop phenomena in freeway networks. *Transportation Research Record: Journal of the Transportation Research Board, Transportation Research Board of the National Academies, Washington, DC*, 2013.
- [31] Martin Treiber, Ansgar Hennecke, and Dirk Helbing. Congested traffic states in empirical observations and microscopic simulations. *Physical review E*, 62(2):1805, 2000.
- [32] David Wilkie, Jason Sewall, Weizi Li, and Ming C. Lin. Virtualized traffic at metropolitan scales. *Frontiers in Robotics and AI*, 2:11, 2015.
- [33] Qianwen Chao, Huikun Bi, Weizi Li, Tianlu Mao, Zhaoqi Wang, Ming C. Lin, and Zhigang Deng. A survey on visual traffic simulation: Models, evaluations, and applications in autonomous driving. *Computer Graphics Forum*, 39(1):287–308, 2020.
- [34] Weizi Li, Dong Nie, David Wilkie, and Ming C. Lin. Citywide estimation of traffic dynamics via sparse GPS traces. *IEEE Intelligent Transportation Systems Magazine*, 9(3):100–113, 2017.
- [35] Weizi Li, David Wolinski, and Ming C. Lin. City-scale traffic animation using statistical learning and metamodel-based optimization. *ACM Trans. Graph.*, 36(6):200:1–200:12, 2017.
- [36] Weizi Li, Meilei Jiang, Yaoyu Chen, and Ming C. Lin. Estimating urban traffic states using iterative refinement and wardrop equilibria. *IET Intelligent Transport Systems*, 12(8):875–883, 2018.
- [37] Lei Lin, Weizi Li, and Srinivas Peeta. Efficient data collection and accurate travel time estimation in a connected vehicle environment via real-time compressive sensing. *Journal of Big Data Analytics in Transportation*, 1(2):95–107, 2019.
- [38] Lei Lin, Weizi Li, and Lei Zhu. Data-driven graph filter based graph convolutional neural network approach for network-level multi-step traffic prediction. *Sustainability*, 14(24):16701, 2022.
- [39] Weizi Li, David Wolinski, and Ming C. Lin. ADAPS: Autonomous driving via principled simulations. In *IEEE*

International Conference on Robotics and Automation (ICRA), pages 7625–7631, 2019.

- [40] Lei Lin, Weizi Li, Huikun Bi, and Lingqiao Qin. Vehicle trajectory prediction using LSTMs with spatial-temporal attention mechanisms. *IEEE Intelligent Transportation Systems Magazine*, 14(2):197–208, 2022.
- [41] Bibek Poudel and Weizi Li. Black-box adversarial attacks on network-wide multi-step traffic state prediction models. In *IEEE International Conference on Intelligent Transportation Systems (ITSC)*, pages 3652–3658, 2021.
- [42] Yu Shen, Laura Zheng, Manli Shu, Weizi Li, Tom Goldstein, and Ming C. Lin. Gradient-free adversarial training against image corruption for learning-based steering. In *Advances in Neural Information Processing Systems (NeurIPS)*, pages 26250–26263, 2021.
- [43] Michael Villarreal, Bibek Poudel, Ryan Wickman, Yu Shen, and Weizi Li. Autojoin: Efficient adversarial training for robust maneuvering via denoising autoencoder and joint learning. 2022.
- [44] Lei Lin, Feng Shi, and Weizi Li. Assessing inequality, irregularity, and severity regarding road traffic safety during covid-19. *Scientific Reports*, 11(13147), 2021.
- [45] Lei Lin, Weizi Li, and Srinivas Peeta. Predicting station-level bike-sharing demands using graph convolutional neural network. In *Transportation Research Board 98th Annual Meeting (TRB)*, 2019.